The second Hopf bifurcation in lid-driven square cavity*

Tao Wang(王涛)[1,2], Tiegang Liu(刘铁钢)[1,†], and Zheng Wang(王正)[3]

[1] LIMB and School of Mathematical Science, Beihang University, Beijing 100191, China
[2] School of Mathematics and Information Science, North Minzu University, Yinchuan 750021, China
[3] Wuhan Maritime Communication Research Institute, Wuhan 430079, China

(Received 5 October 2019; revised manuscript received 3 December 2019; accepted manuscript online 14 January 2020)

To date, there are very few studies on the second Hopf bifurcation in a driven square cavity, although there are intensive investigations focused on the first Hopf bifurcation in literature, due to the difficulties of theoretical analyses and numerical simulations. In this paper, we study the characteristics of the second Hopf bifurcation in a driven square cavity by applying a consistent fourth-order compact finite difference scheme recently developed by us. We numerically identify the critical Reynolds number of the second Hopf bifurcation located in the interval of $(11093.75, 11094.3604)$ by bisection. In addition, we find that there are two dominant frequencies in its spectral diagram when the flow is in the status of the second Hopf bifurcation, while only one dominant frequency is identified if the flow is in the first Hopf bifurcation via the Fourier analysis. More interestingly, the flow phase portrait of velocity components is found to make transition from a regular elliptical closed form for the first Hopf bifurcation to a non-elliptical closed form with self-intersection for the second Hopf bifurcation. Such characteristics disclose flow in a quasi-periodic state when the second Hopf bifurcation occurs.

Keywords: unsteady lid-driven cavity flows, second Hopf bifurcation, critical Reynolds number, numerical simulation

PACS: 05.45.Pq, 05.70.Jk **DOI:** 10.1088/1674-1056/ab6b15

1. Introduction

The two-dimensional (2D) flows in driven cavities have been extensively studied in the past 60 years,[1–7] starting from the pioneering work by Kawaguti. Among them, several works have contributed to establish a clear picture of the steady solutions to the problems for Reynolds numbers up to several thousands, mainly by employing vorticity–velocity and biharmonis solvers.[2,4,6]

In recent decades, scientists have shifted their research focus on studying the first Hopf bifurcation,[8–10] in which the flow transfers its stationary state to non-stationary periodic state. In literature, there are majorally two kinds of methods applied to study the first Hopf bifurcation. One is through theoretical analyses, the other is via numerical simulations. The first attempt was made by Hou *et al.*,[8] who numerically predicted that the critical Reynolds number of Re_{c1} was larger than 7500 for the occurrence of the first Hopf bifurcation with a lattice Boltzmann method. Immediately, Poliashenko and Aidun[9] confirmed the prediction of Hou *et al.* and gave out $Re_{c1} = 7763 \pm 2\%$ by a low order finite element method. It seems true that the critical Reynolds number of the first Hopf bifurcation is beyond 7500 both from theoretical analysis and numerical simulation. In theoretical analysis, Fortin *et al.*[11] predicted the critical Reynolds number of $Re_{c1} = 8000$ for the first Hopf bifurcation, through an eigenvalue analysis of the linearized Navier–Stokes equations by means of a finite element spatial discretization. Late, Cazemier *et al.*[12] found Re_{c1} was at 7819.0 through the eigenvalue analysis of the linearized Navier–Stokes equations but with a proper orthogonal decomposition to solve the linearized system. On the numerical side. Auteri *et al.*[13] applied a singularity subtraction technique and second-order spectral projection method to locate the Re_{c1} was in the interval $(8017.6, 8018.8)$. They claimed that an asymptotic solution existed when Reynolds number was less than Re_{c1} and the asymptotic solution would become periodic when Reynolds number was larger than Re_{c1}. More recently, Bruneau *et al.*[10] calculated Re_{c1} was in the interval $(8000, 8050)$ by a third-order Murman-like scheme.

With the increase of Reynolds number, the flow experiences transition from the first Hopf bifurcation to the second Hopf bifurcation, where the flow is supposed to be under a quasi-periodic state. Due to the second bifurcation is a further bifurcation of flow instability, it is very difficult to get useful information under the frame of eigenvalue analysis of the linearized Navier–Stokes equations. To date, one can only use numerical simulations to make investigation and very few results disclosed. Auteri *et al.*[13] numerically forecasted the second Hopf bifurcation with a critical Reynolds number, Re_{c2}, located in the interval of $(9685, 9765)$. Because the flow instability starts from the wall boundary layer, where it becomes very thinner under a high Reynolds number. To predict the second bifurcation, the boundary layer has to be resolved

*Project supported by the National Natural Science Foundation of China (Grant Nos. 11601013 and 91530325).
†Corresponding author. E-mail: liutg@buaa.edu.cn
© 2020 Chinese Physical Society and IOP Publishing Ltd

accurately with either very fine mesh or high order numerical method. This makes the numerical simulation very costly and challenging. In even worse case, recently, it was found by us[14] that a high order method might suffer numerical instability inside the wall boundary layer if a lower order treatment of boundary conditions is equipped. Such lower order techniques of wall treatment are very popular in applications of high order numerical methods. To fix this problem, we have developed a consistent fourth-order compact finite difference scheme,[14] in which both the order of accuracy and major truncation error term are kept the same for the inner and boundary schemes. Such a high order scheme can efficiently suppress the numerical instability insider the wall boundary layer.

In this work, we will apply the consistent fourth-order compact finite difference scheme to study the characteristics of the second Hopf bifurcation in the driven square cavity. In addition, we employ bisection to locate the critical Reynolds number and analyze the characteristics of the second Hopf bifurcation with Fourier analysis and phase diagram. We discover that the flow phase portrait makes transition from a regular elliptical closed form for the first Hopf bifurcation to a non-elliptical closed form with self-intersection when the second Hopf bifurcation occurs, indicating a quasi-periodic flow behavior.

2. Model description and numerical methods

2.1. Governing equations

In this paper, the 2D lid–driven cavity problems are considered and governed with the 2D incompressible Navier–Stokes equations given in the non-dimensional vorticity–stream function in the form as

$$\psi_{xx}+\psi_{yy}=-\xi, \tag{1}$$

$$\xi_t+u\xi_x+v\xi_y=\frac{1}{Re}(\xi_{xx}+\xi_{yy}), \tag{2}$$

where u and v are the velocity components in x and y directions, respectively, Re is the Reynolds number and $u=\psi_y$, $v=-\psi_x$. Equation (1) is referred to as the stream function equation, equation (2) is referred to as the vorticity equation.

The computational domain is set to $\{(x,y)|0\le x\le 1, 0\le y\le 1\}$. The boundary conditions are given as follows:

$$\begin{cases} y=1: & u=1,\ v=0,\ \psi=0,\\ y=0: & u=0,\ v=0,\ \psi=0,\\ x=0,1: & u=0,\ v=0,\ \psi=0. \end{cases}$$

Because the vorticity on the wall is unknown, in the process of solving the Eq. (2), the condition of vorticity on the boundary must be supplemented. In this paper, the numerical boundary conditions of vorticity in Ref. [15] are used, namely,

$$h(6\xi_1+4\xi_2-\xi_3)/21+o(h^4)$$

$$=(15\psi_1-16\psi_2+\psi_3)/(14h)\pm V_w,$$

where the subscripts 1, 2, 3 represent the boundary points, its neighbor, and sub-neighbor points, respectively. V_w is the tangential velocity of the wall. On the sliding wall, $V_w=1$. On the solid wall, $V_w=0$.

In Fig. 1, the typical flow pattern in a driven cavity is illustrated, where there is a primary vortex (PV) at the center, three corner vortexes locate respectively at the bottom (bottom left vortex (BL), bottom right vortex (BR), and the top (top left vortex (TL)).

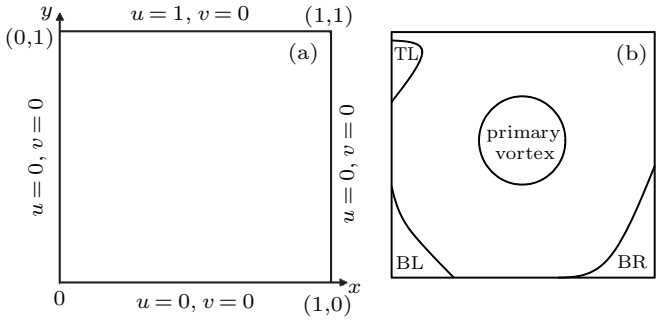

Fig. 1. The lid-driven cavity problem: (a) boundary condition and (b) the schematic diagram.

2.2. Numerical methods

The numerical method employed in this work is the consistent fourth-order compact finite difference scheme developed by Wang *et al.*[14] One can refer to Ref. [14] for details. After the spatial discretization with the consistent fourth-order compact finite difference scheme, an explicit third-order TVD Runge–Kutta scheme (for details see Ref. [16]) was used to do time discretization.

Mesh convergency for the numerical method has been carried out with a driven square cavity with $Re=10000$. Table 1 shows the amplitude values and periodic lengths of the u-velocity when the fluid reaches the periodic state ($t=2000$) using three uniform meshes (65×65,129×129 and 257×257) at $Re=10000$. It can be seen that the results under grid 129×129 are in good agreement with those under fine grid 257×257 and the maximum error is less than 1%.

Table 1. Comparison of the amplitude values and periodic lengths of the u-velocity when the fluid reaches the periodic state at $Re=10000$.

Grid points	Amplitude value	Error/%	Periodic lengths	Error/%
65×65	0.000137	1.481	1.806	0.6600
129×129	0.000135	0.735	1.818	0.0549
257×257	0.000136	–	1.819	–

Based on the mesh convergences test of the above benchmark simulation, in this paper, we take the time step size of $\Delta t=1\times10^{-3}$ and solve the system with 129×129 uniform grids in the numerical simulations.

3. Results and discussion

We determine the different states of the flow according to the time evolution of velocity at a fixed point $(x,y)=(0.5,0.5)$ of the cavity.

3.1. The critical Reynolds number of the second Hopf bifurcation

From the introduction, it is known that the flow in a driven square cavity becomes periodic when the Reynolds number is larger than a critical number of Re_{c1}, which is beyond 7500. We confirmed that the flow at $Re=10000$ is still periodic in its first Hopf bifurcation as done by Tian *et al.*[17] We calculated the flow with a higher $Re=12500$ for t from 0 to 3000 as shown in Figs. 2(a) and 3(a) for the evolution of u-velocity and v-velocity at the geometric center point. We give the enlarged Figs. 2(a) and 3(a) for t from 2960 to 3000 and found that the flow was under quasi-period as shown in Figs. 2(b) and 3(b) for the evolution of u-velocity and v-velocity at the geometric center point. From the enlarged figures, one can see that the flow from the initial unstable state converges eventually into a quasi-periodic state.

As a result, the critical Reynolds number of Re_{c2} is located in between $Re=10000$ and $Re=12500$. Now, we find the Re_{c2} via bisection. Starting from $a_0=10000$, $b_0=12500$, if at $Re=(a_k+b_k)/2$, we get periodic solution, then we let $a_k=(a_k+b_k)/2$; If at $Re=(a_k+b_k)/2$, we get quasi-periodic solution, then we let $b_k=(a_k+b_k)/2$. We repeat this process and carry out the dichotomy for 12 times, and then we obtain a very small interval. Finally, in this way, the Re_{c2} has been localized in the small interval $(11093.75, 11094.3604)$. Table 2 shows the process of localizing the range of the Re_{c2} by bisection.

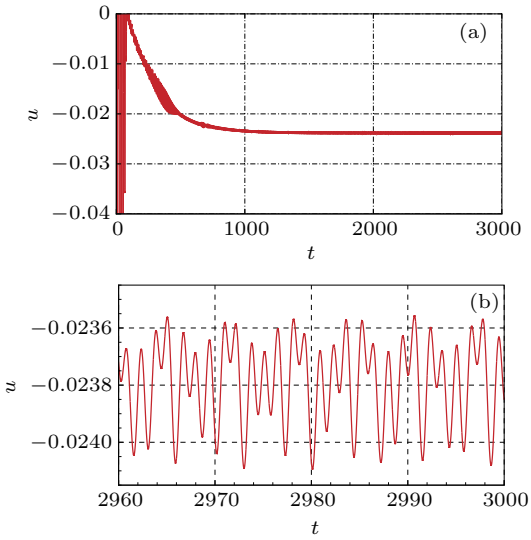

Fig. 2. The time history of u-velocity for $Re=12500$: (a) total time; (b) local time.

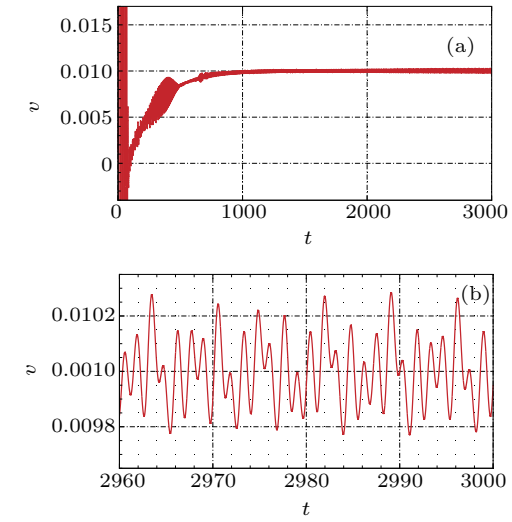

Fig. 3. The time history of v-velocity for $Re=12500$: (a) total time; (b) local time.

Table 1. The process of bisection for confirming Re_{c2}.

k	a_k	b_k	$(a_k+b_k)/2$	Solution	Re_{c2}
0	10000	12500	11250	quasi-periodic	(11250, 12500)
1	10000	11250	10625	periodic	(10625, 11250)
2	10625	11250	10937.5	periodic	(10937.5, 11250)
3	10937.5	11250	11093.75	periodic	(11093.75, 11250)
4	11093.75	11250	11171.875	quasi-periodic	(11093.75, 11171.875)
5	11093.75	11171.875	11132.8125	quasi-periodic	(11093.75, 11132.8125)
6	11093.75	11132.8125	11113.2812	quasi-periodic	(11093.75, 11113.2812)
7	11093.75	11113.2812	11103.5156	quasi-periodic	(11093.75, 11103.5156)
8	11093.75	11103.5156	11098.6328	quasi-periodic	(11093.75, 11098.6328)
9	11093.75	11098.6328	11096.1914	quasi-periodic	(11093.75, 11096.1914)
10	11093.75	11096.1914	11094.9707	quasi-periodic	(11093.75, 11094.9707)
11	11093.75	11094.9707	11094.3604	quasi-periodic	(11093.75, 11094.3604)

In a series of Figs. 4 and 5 we present the time history of $u(t)$ for different Reynolds numbers. In these graphes, we can clearly see that during the process of determining the critical Reynolds number, the function $u(t)$ solution is either periodic or quasi-periodic.

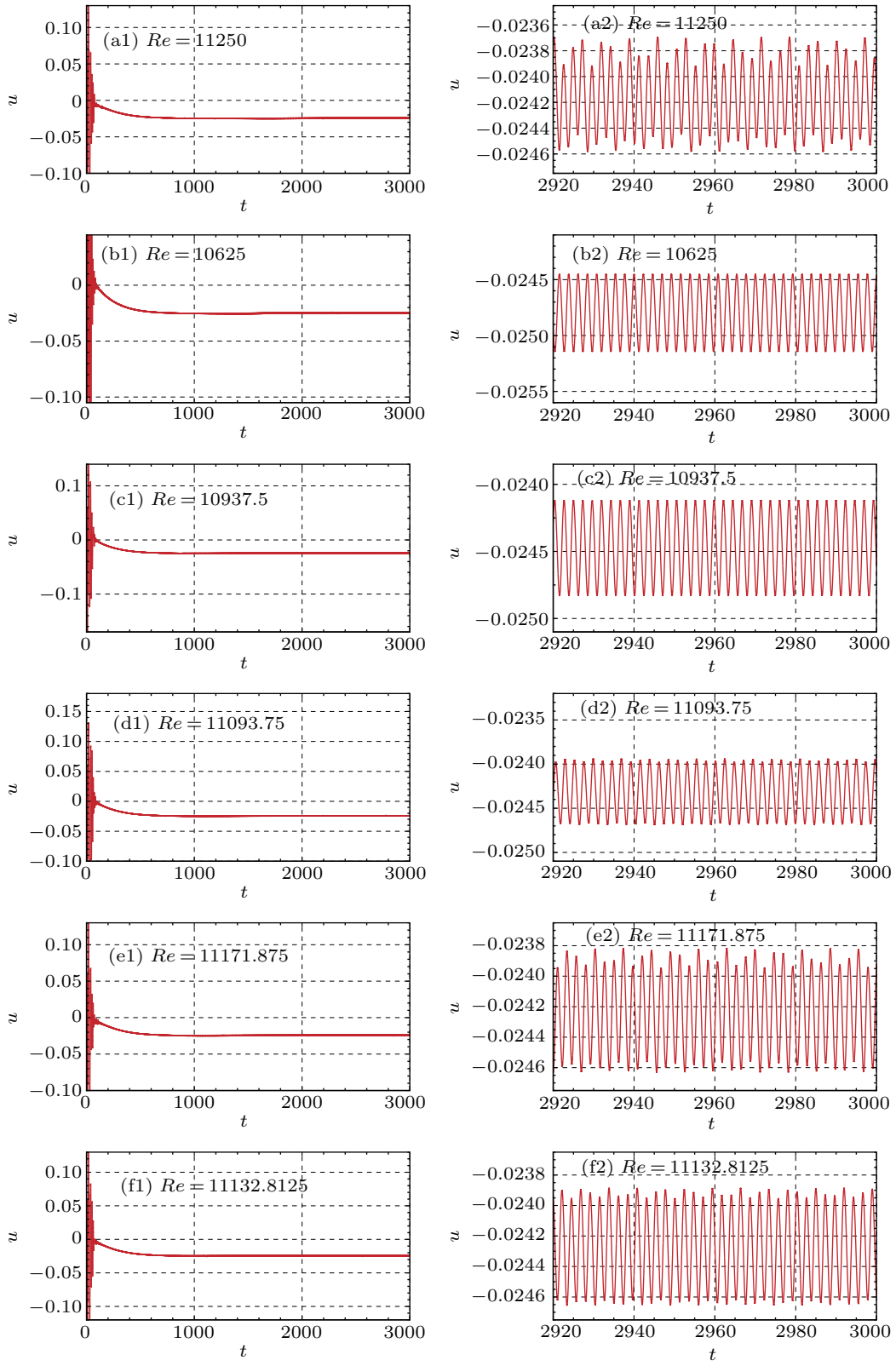

Fig. 4. The time history of u-velocity for different Reynolds numbers: (a1)–(f1) total time, (a2)–(f2) local time.

3.2. The analysis of second Hopf bifurcation

We analyze the flow behavior from the time history of flow velocity, its spectrum and phase diagram for two specific Reynolds numbers of $Re = 10000$, 12500. For the former, the flow is in the status of its first Hopf bifurcation, for the latter the flow is in its second Hopf bifurcation. Since the properties of u-velocity and v-velocity are the same, we only look at the behavior of the u-velocity. In this way, we may have a clear understanding of the nature of the second bifurcation.

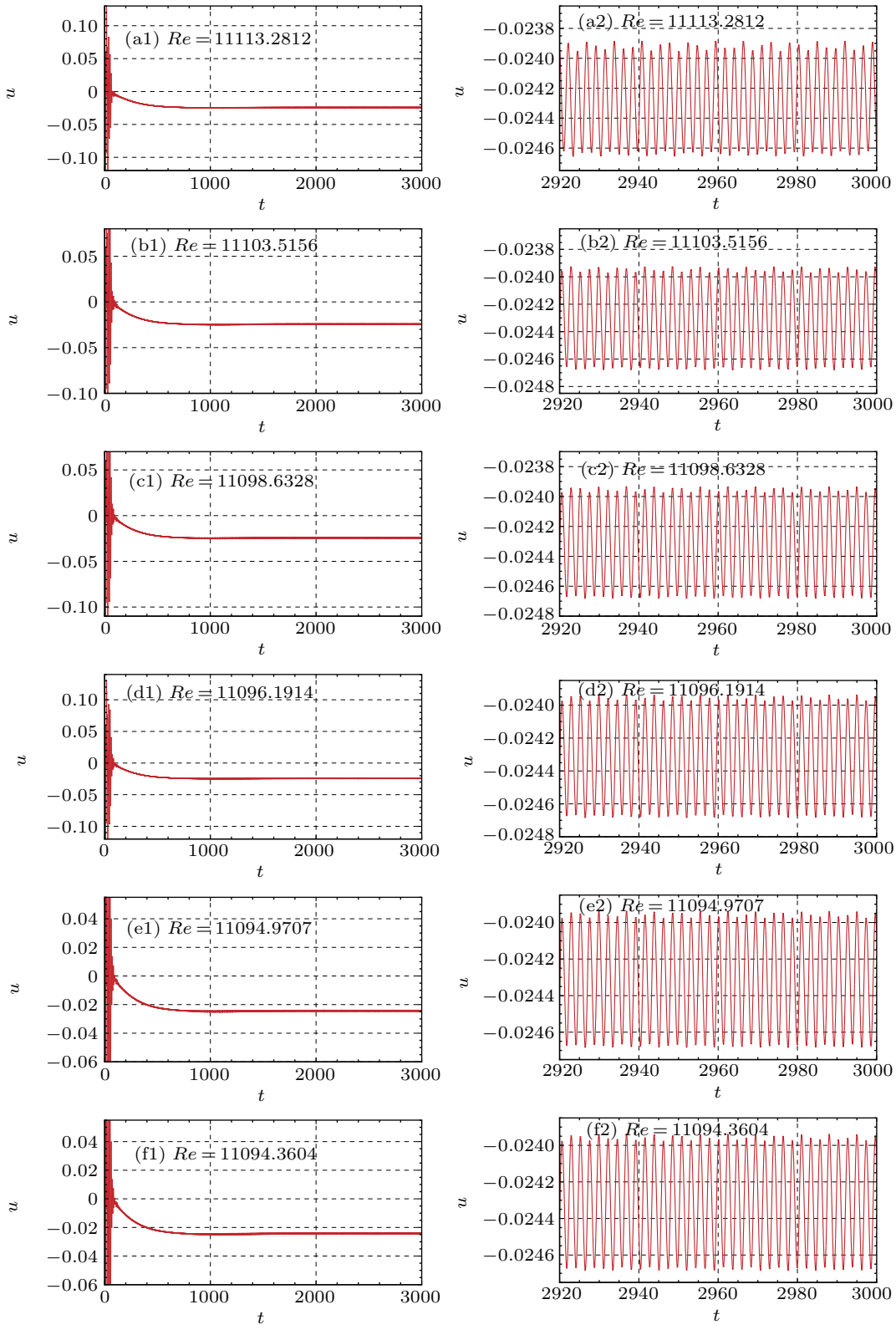

Fig. 5. The time history of u-velocity for different Reynolds numbers: (a1)–(f1) total time, (a2)–(f2) local time.

Figures 6(a) and 6(b) show their time histories of u-velocity for the respective $Re = 10000$ and $Re = 12500$; the solutions clearly exhibit periodic behaviors with non-dimensional periodic lengths of $\tau = 1.818$ for the former and $\tau = 1.429$ for the latter.

The flow behaviors looks very different from Figs. 6(a) and 6(b). We took Fourier analysis from $t = 2960$ to $t = 2970$. The results are shown in Figs. 7(a) and 7(b) for the power spectrum density of $u(t)$ for the respective $Re = 10000$ and $Re = 12500$. There is only one frequency of $f = 0.55005$

found for the flow at $Re = 10000$, while there are two distinct frequencies for the flow at $Re = 12500$, one with a frequency of $f_1 = 0.38654$ and the other with a frequency of $f_2 = 0.77309$. This show that the flow at $Re = 10000$ is periodic, while it is in the quasi-periodic behavior at $Re = 12500$.

We further plotted the phase portraits by using the delay coordinates $u(t)$ and $u(t+\tau)$ with $\tau = 1.818$ for $Re = 10000$ and $\tau = 1.429$ for $Re = 12500$, respectively. The results are shown in Figs. 8(a) and 8(b). One can observe that a perfect elliptic cycle formed for $Re = 10000$, while a non-ellipse closed pattern formed with self-intersection for $Re = 12500$. These features further confirms that the flow is in stable period under the first Hopf bifurcation and in quasi-period for the second Hopf bifurcation.

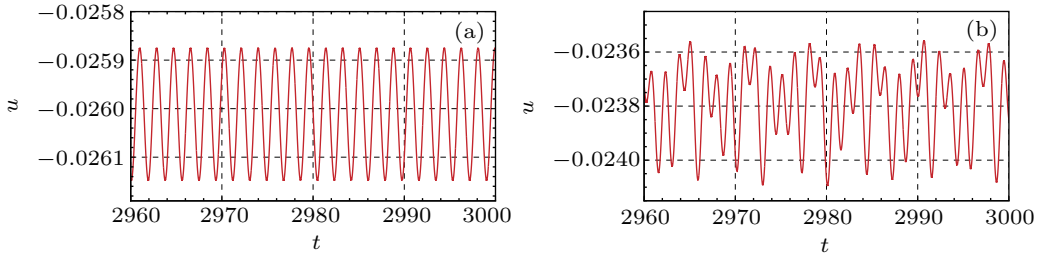

Fig. 6. The local time history of u-velocity for (a) $Re = 10000$ with $\tau = 1.818$ and (b) $Re = 12500$, $\tau = 1.429$.

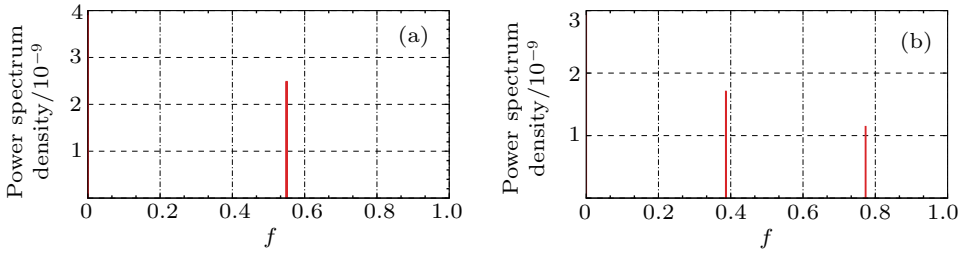

Fig. 7. The u-velocity power spectrum density of $u(t)$ for (a) $Re = 10000$ and (b) $Re = 12500$.

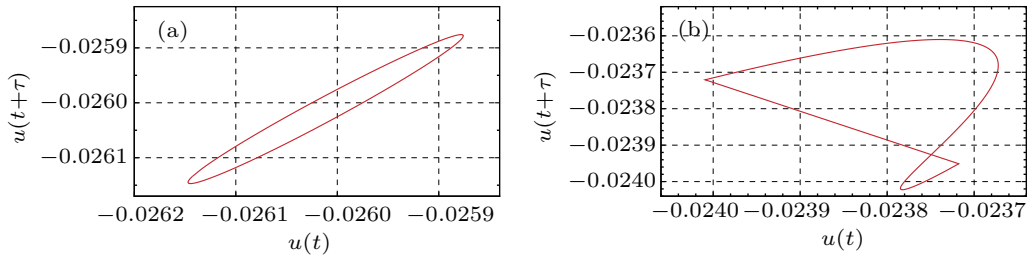

Fig. 8. Phase portrait of $u(t)$ for (a) $Re = 10000$, $\tau = 1.818$ and (b) $Re = 12500$, $\tau = 1.429$.

In all, when $Re \in (10000, Re_{c2})$, the flow state is periodic, which is similar to that for $Re = 10000$ although the periodic value is different for different Re. And when $Re \in (Re_{c2}, 12500)$, the flow state is quasi-periodic, which is similar to that for $Re = 12500$ although the two frequencies are different for different Re.

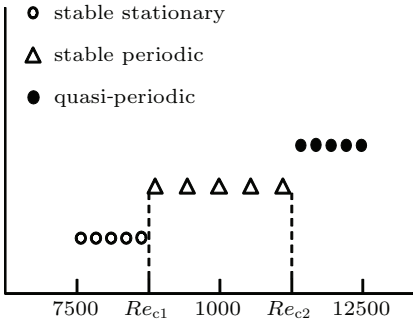

Fig. 9. Bifurcation diagram.

Finally, we plot the findings in Fig. 9 to give a qualitative summary. The flow is stationary below Re_{c1}, periodic in $Re \in (Re_{c1}, Re_{c2})$, and quasi-periodic in $Re \in (Re_{c2}, 12500)$.

4. Conclusion

In this paper, we investigated the flow properties under its second Hopf bifurcation in a driven square cavity by applying a consistent fourth-order compact finite difference scheme. We have located the critical Reynolds number of the second Hopf bifurcation in a very narrow interval of $(11093.75, 11094.3604)$. Moreover, by analyzing the spectrum and phase portrait, we found that there are two dominant frequencies and the phase portrait changes from an ellipse closed form to the non-ellipse closed form, when the flow is in the status of the second Hopf bifurcation. We conjecture that the flow might experience further bifurcation before it be-

comes turbulent. This will be our future work.

Acknowledgment

The authors thank Professor Y B Ge in the Ning-xia University for helpful discussion and the valuable suggestions of the reviewers.

References

[1] Kawaguti M 1961 *J. Phys. Soc. Jpn.* **16** 2307
[2] Erturk E 2006 *Int. J. Numer. Meth. Fluids* **50** 421
[3] Das M K and Kanna P 2007 *International Journal of Numerical Methods for Heat and Fluid Flow* **17** 799
[4] Erturk E 2009 *Int. J. Numer. Meth. Fluids* **60** 275
[5] Tang J S, Zhao M H, Han F and Zhang L 2011 *Chin. Phys. B* **20** 020504
[6] Nuriev A N, Egorov A G and Zaitseva O N 2016 *Fluid Dyn. Res.* **48** 61405
[7] Fang L and Ge M W 2017 *Chin. Phys. Lett.* **34** 030501
[8] Hou S, Zou Q, Chen S, Doolen G and Cogley A C 1995 *J. Comput. Phys.* **118** 329
[9] Poliashenko M and Aidun A 1995 *J. Comput. Phys.* **121** 246
[10] Bruneau C H and Saad M 2006 *Comput. Fluids* **35** 326
[11] Fortin A, Jardak M, Gervais J and Pierre R 1997 *Int. J. Numer. Method Fluids* **24** 1185
[12] Cazemier W, Verstappen R and Veldman A 1998 *Phys. Fluids* **10** 1685
[13] Auteri F, Parolini N and Quartapelle L 2002 *J. Comput. Phys.* **183** 1
[14] Wang T and Liu T G 2019 *Numer. Math.: Theory, Methods and Applications* **12** 312
[15] Spotz W F 1998 *Int. J. Numer. Method Fluids* **28** 737
[16] Shu C W and Osher S 1988 *J. Comput. Phys.* **77** 439
[17] Tian Z F, Liang X and Yu P 2011 *Int. J. Numer. Method Eng.* **88** 511